Published in final edited form as:

J Mater Chem C Mater. 2018 October 14; 6(38): 10263–10269. doi:10.1039/C8TC02671H.

Enhancing the Tactile and Near-Infrared Sensing Capabilities of Electrospun PVDF Nanofibers with the Use of Gold Nanocages

Haoxuan Li[a,b], **Tong Wu**[a], **Minghao Xie**[c], **Yifeng Shi**[d], **Song Shen**[a], **Ming Zhao**[c], **Xuan Yang**[a], **Legna M. Figueroa-Cosme**[c], **Qinfei Ke**[b], and **Younan Xia**[a,c,d]

[a]The Wallace H. Coulter Department of Biomedical Engineering, Georgia Institute of Technology and Emory University, Atlanta, GA 30332, USA

[b]Key Laboratory of Textile Science and Technology, College of Textiles, Donghua University, Shanghai 201620, P. R. China

[c]School of Chemistry and Biochemistry, Georgia Institute of Technology, Atlanta, GA 30332, USA

[d]School of Chemical and Biomolecular Engineering, Georgia Institute of Technology, Atlanta, GA 30332, USA

Abstract

Owing to its piezoelectric and pyroelectric properties, poly(vinylidene fluoride) (PVDF) has been extensively explored for applications related to tactile sensing, energy harvesting, and thermal imaging. However, PVDF cannot be directly used to detect light because of its weak absorption in the visible and near-infrared (NIR) regions, preventing effective conversion from light to heat and then electrical signal. In this work, we address this issue by incorporating Au nanocages (AuNCs) into PVDF nanofibers during electrospinning. The strong and tunable optical absorption associated with AuNCs makes them an effective transducer for converting light to heat and then electrical signal. The presence of AuNCs and the strong electric field inherent to electrospinning both promote the formation of the ferroelectric β phase for maximal piezoelectric and pyroelectric conversions. With the incorporation of AuNCs, the electrospun PVDF nanofibers show enhanced capabilities for tactile and NIR sensing. While the voltage output under the tactile force is increased by 12.6-fold relative to the case of pristine PVDF nanofibers, a voltage output of 7.2 V is achieved when the hybrid device is subjected to the on/off cycles of NIR irradiation by an 808-nm diode laser at a power density of 0.2 W/cm^2.

Table of Contents

younan.xia@bme.gatech.edu.

Conflicts of interest

The authors declare no competing financial interest.

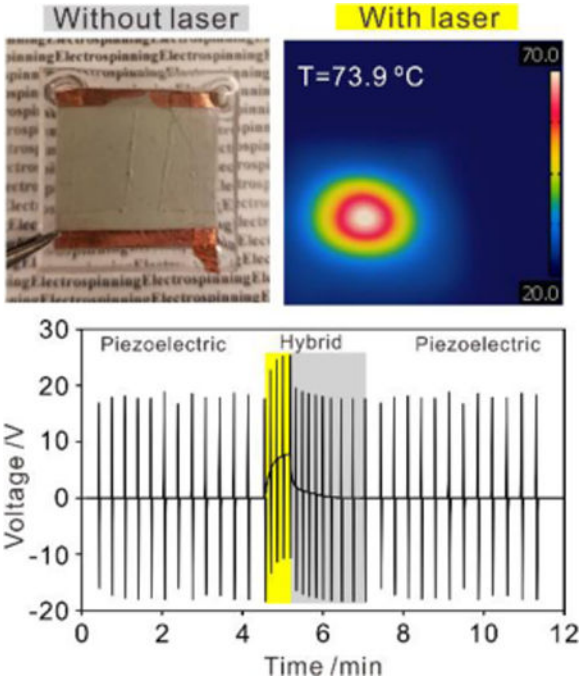

The incorporation of AuNCs into PVDF nanofibers by electrospinning for enhancing the performance of tactile and near-infrared sensing

Introduction

Plasmonic nanomaterials have been extensively explored for applications ranging from photonics to medical diagnostics because of their localized surface plasmon resonance (LSPR) and related properties.[1] To this end, Au-based nanostructures with a wide variety of non-spherical shapes or complex structures have been developed to provide tunable LSPR peaks in the visible and near-infrared (NIR) regions.[2] Among them, Au nanocages (AuNCs) with hollow interiors and porous walls have received particular attention as their LSPR is typically dominated by absorption rather than scattering, and the peak position can be precisely tuned to any wavelength of interest in the range of 400−1200 nm by controlling the wall thickness relative to the overall dimensions.[2] Empowered by their strong absorption of light, AuNCs can serve as a photothermal transducer to effectively convert photons to phonons or heat.[3] In principle, one can incorporate AuNCs into a pyroelectric material to obtain a hybrid system that can be utilized to fabricate optical detectors or imagers working in the visible and NIR regions.

Poly(vinylidene fluoride) (PVDF) is a good candidate for the pyroelectric component. When poled into the ferroelectric β phase, this polymer shows strong piezoelectric and pyroelectric properties that have been utilized to fabricate tactile sensors and thermal cameras by converting mechanical and thermal energies, respectively, to electrical signal.[4–7] The conventional poling of a PVDF film involves the application of a strong electric field (typically, 300 kV/cm) to the sample while it is held at 70−100 °C.[8–11] In addition, the polymer chains can also be aligned to obtain the β phase when PVDF is dissolved in a

mixture of acetone and N, N-dimethylformamide (DMF), and electrospun into nanofibers by leveraging the strong electrical field and mechanical stretching force associated with electrospinning.[12–14] Moreover, it has been reported that the incorporation of nanoparticles made of materials such as Ag,[15,16] Au,[17–19] and ZnO[20] could play a positive role in aligning the polymer chains and thus enhancing the piezoelectric response. It was proposed that the strong electrostatic interactions between the positively charged nanoparticles and the negatively charged fluorine atoms in the polymer backbone could produce interfacial polarization on the crystalline phase to facilitate the formation of the β phase.[13]

Herein, we demonstrate the capability of directly incorporating AuNCs into PVDF nanofibers during an electrospinning process for the fabrication of tactile sensors and NIR detectors with greatly enhanced sensing performance. The presence of AuNCs not only facilitates the formation of the desired ferroelectric β phase but also enables a unique feature for converting NIR light to heat and then electrical signal, allowing the hybrid nanomaterial to simultaneously respond to mechanical and optical stimulations. To fully demonstrate the potential of such a hybrid material, we compare the piezoelectric, pyroelectric, and coupled outputs in terms of electrical signal when the device is subjected to the tactile force, NIR irradiation, and a combination of both, with the pristine PVDF nanofibers serving as a reference.

Experimental section

Chemicals and materials

Silver trifluoroacetate (CF_3COOAg), sodium hydrosulfide (NaHS), hydrochloric acid (HCl), gold(III) chloride trihydrate ($HAuCl_4{\cdot}3H_2O$), acetone, N, N-dimethylformamide (DMF), poly(vinylpyrrolidine) (PVP, $M_w{\approx}55{,}000$), and poly(vinylidene fluoride) (PVDF, $M_w{\approx}275{,}000$) were all obtained from Sigma-Aldrich (St. Louis, MO, USA). Ethylene glycol (EG) was obtained from J. T. Baker (Center Valley, PA, USA). Sylgard 184 silicone elastomer kit (PDMS) was purchased from Dow Corning (Midland, MI, USA), and the plastic films pre-coated with indium tin oxide (ITO) were ordered from Kaivo Optoelectronic Technology (Zhuhai, Guangzhou, China).

Preparation of nonwoven mats made of AuNC/PVDF nanofibers

We prepared the AuNCs as described in a previous report.[21] The solution for electrospinning was prepared by dissolving PVDF in a mixture of acetone and DMF (v/v = 3:7) at a final concentration of 18 wt.%. The AuNCs were dispersed in DMF at a weight percentage of 0.01% to PVDF and then added into the PVDF solution to obtain a homogeneous mixture. The mixture was loaded into a 5-mL plastic syringe with a 21-gauge needle attached and dispensed using a syringe pump. The injection rate was maintained at 1 mL/h. A voltage of 15 kV was applied, while the distance between the tip of the needle and the collector was set to 15 cm.

Fabrication of devices using the AuNC/PVDF nanofibers

A nonwoven mat of the AuNC/PVDF nanofibers was cut into small pieces with an area of $1.5 \times 1.5\ cm^2$. It was sandwiched between two pieces of thin plastic films pre-coated with

ITO. The sandwich structure was then sealed with PDMS, an elastomer that allowed the device to recover its original structure effectively after the bending stress was released.

Characterization

The morphologies of the nanofiber mats were examined using an SU-8230 field-emission scanning electron microscope (Hitachi, Japan). The average diameter of the nanofibers was derived from 100 fibers on the scanning electron microscopy (SEM) images using Adobe Acrobat X Pro (ADOBE, USA). Transmission electron microscopy (TEM) images were taken on a HT7700 microscope (Hitachi, Japan) operated at 120 kV. For AuNCs, the sample was prepared by placing a drop of the particles suspended in water on a carbon-coated copper grid, followed by drying under ambient conditions. For AuNC/PVDF nanofibers, the sample was prepared by directly collecting the fibers with a carbon-coated copper grid. The weight percentage of AuNCs was determined using a NexION 300Q inductively-coupled plasma mass spectrometer (ICP-MS, PerkinElmer, USA). X-ray diffraction (XRD) patterns and Fourier transform infrared (FT-IR) spectra in the attenuated total reflection (ATR) mode were obtained using an X'Pert PRO Alpha-1 diffractometer (PANalytical, The Netherlands) and a Varian 640 infrared spectrophotometer (Agilent Technologies, USA), respectively. Absorption spectra were recorded using a Cary 60 spectrometer (Varian, USA). An 808-nm diode laser coupled to a 100-μm-core nanofiber (Power Technology, USA) was used as the light source. The outputs in terms of open circuit voltage and current were recorded at different frequencies using a CHI 600E electrochemical workstation (CH Instruments, USA).

Discrete dipole approximation (DDA) calculation

The nanocage was approximated as a nanobox, which was generated by *i*) creating a cube and *ii*) subtracting a smaller cube from the interior to create a box, as described in previous reports.[22–24] Once the shape was generated and inspected with Visual Molecular Dynamics (VMD) 1.9.2, it was uploaded as a shape-file into the ddscat 7.2.0 software. In all cases, the propagation (k-vector) and electric field (E_x and E_y-field) of the incident photon were perpendicular and parallel, respectively, to the (100)-facet of the cubic box, as indicated in Fig. S2. Furthermore, in all simulations, dipoles between 10^4 and 10^5 were used to ensure accurate results. The dielectric constant of a $Au_{0.52}Ag_{0.48}$ alloy was taken from reference 25. Since all spectra were measured when the nanocages were suspended in water, the dielectric constants of the surrounding medium and the interior space were taken to be $\varepsilon_m = n^2 = 1.78$.

Results and discussion

The TEM image in Fig. 1A indicates that the AuNCs had a well-defined hollow interior, together with an average outer edge length of about 53 nm and a wall thickness of approximately 8.5 nm. The LSPR peak position of AuNCs is mainly determined by their size and wall thickness, as well as the dielectric constant of the surrounding medium. In the current study, we focused on AuNCs with LSPR peaks tuned to the NIR region. As confirmed by the UV-vis-NIR spectrum in Fig. 1B, the LSPR peak of the AuNCs in an aqueous suspension was positioned at 787 nm, close to the output wavelength (808 nm) of the diode laser used for photothermal heating. Since the absorption spectrum of AuNCs

depends on their surrounding environment, we also measured the absorption spectrum derived from an aqueous suspension of the AuNC/PVDF nanofibers. Relative to the LSPR peak of the AuNCs in an aqueous suspension, only a slight red shift of about 21 nm was observed for the peak in the case of AuNC/PVDF nanofibers (Fig. S1), confirming that the LSPR spectrum of AuNCs would not be changed significantly when the surrounding medium was switched from water to PVDF. For the AuNC/PVDF nanofibers, the strong absorption in the range of 300−500 nm can be attributed to PVDF and/or the nanofiber morphology.[17]

To verify the optical properties of the AuNCs, we also calculated the absorption and scattering cross-sections of one individual AuNC using the DDA method.[26] We modeled the nanocage with an alloy composition composed of 52% Au and 48% Ag based on the ICP-MS data, and assumed that it was surrounded by and completely filled with water. The nanocage was further simplified as a nanobox, together with an outer edge length of 54 nm and a wall thickness of 6 nm. As shown in Fig. S2, the calculated extinction, absorption, and scattering cross sections at resonance are 3.69×10^{-14}, 2.65×10^{-14}, and 1.04×10^{-14} m^2, respectively. The LSPR peak of the AuNC derived from the DDA calculation was located at 767 nm, in reasonable agreement with the peak at 787 nm recorded experimentally.

Fig. 2A shows a photograph of the as-prepared mat of PVDF nanofibers containing AuNCs before it was cut into smaller pieces for device fabrication. The mat showed a light blue tint that matched the color displayed by the aqueous suspension of AuNCs, suggesting that the AuNCs did not aggregate into larger structures during electrospinning. As shown by the SEM images in Fig. 2B, the AuNC/PVDF nanofibers had a smooth surface, together with an average diameter of 434 ± 73 nm. In comparison, the mat of pristine PVDF nanofibers showed a white color, and the fibers took an average diameter of 462 ± 72 nm (Fig. 2C and D). These results suggest that the inclusion of AuNCs did not cause any major changes to the electrospinning process. The AuNCs dispersed in the PVDF nanofibers could be readily resolved under a TEM image (see the inset in Fig. 2B), confirming the absence of aggregation. Fig. 2E shows a schematic drawing of the device. To facilitate electrical measurements and protect the device from repeated compressive deformation, the nonwoven mat (1.5×1.5 cm^2 in area) of PVDF nanofibers containing AuNCs at a weight percentage of 0.01% was sandwiched between two plastic films pre-coated with ITO. As shown by the photograph in the inset of Fig. 2E, the as-fabricated device had a total thickness of about 1 mm. It was flexible and could be controllably bent without cracking. The good transparency of ITO and PDMS, with a transmittance as high as 84% in the visible and NIR regions, allowed the light to easily reach the layer of PVDF nanofibers without significant attenuation.

We used both XRD and FT-IR spectroscopy to analyze the crystal phases of AuNC/PVDF and PVDF in the form of nonwoven mats of nanofibers. In Fig. 3A, the diffraction patterns of both AuNC/PVDF and PVDF nanofibers show relatively weak peaks at $2\theta = 18.5°$ and 26.6° (corresponding to the diffractions from the α phase). Instead, both samples showed a strong diffraction peak at 20.4° to confirm the dominance of the β phase, which is crucial for both piezoelectric and pyroelectric applications.[27] The peak intensity ratio between the β and α phases was increased from 1.55 for PVDF to 1.76 for AuNC/PVDF nanofibers,

demonstrating the enrichment of the β phase in the case of AuNC/PVDF nanofibers relative to the pristine sample. Fig. 3B compares FT-IR spectra collected from the samples. The vibrational bands at 840 cm^{-1} (CH_2, CF_2 rocking and asymmetrical stretching) and 1276 cm^{-1} are characteristic of the β phase, while the α phase should exhibit two peaks at 764 [CF_2 bending and skeletal bending of (C(F)-C(H)-C(F))] and 976 cm^{-1} (CH_2 rocking).[16,19] It is also worth noting that the intensities of the peaks corresponding to the α phase were suppressed, and those for the peaks corresponding to the β phase were enhanced for the AuNC/PVDF nanofibers. The content of β phase in the nanofibers could be estimated using the equation $F(\beta) = A_\beta / (1.3A_\alpha + A_\beta)$, where A_α and A_β are the absorbance at 764 and 840 cm^{-1}, respectively.[9] The content of β phase in the PVDF nanofibers was increased from 83.5 to 93.2% when AuNCs were added into the solution at a weight percentage of 0.01% for electrospinning. The incorporation of AuNCs in PVDF nanofibers was able to straighten the PVDF backbone, promoting the formation of the β phase instead of the α phase. Besides, the dipole-dipole interactions between PVDF and AuNCs could induce a polymorph change from the α phase to the β phase.[19] Taken together, it can be concluded that the content of the β phase in the AuNC/PVDF nanofibers was greater than that in the pristine PVDF nanofibers.

We first measured the voltage output from a mat of AuNC/PVDF nanofibers when the device was used for tactile sensing (Fig. 4A). When a repeated compressive force was applied to the device, a positive voltage pulse as high as 18.3 V was measured, and a negative voltage pulse appeared as the compressive strain was released. In comparison, the maximum voltage output from a device made of the pristine PVDF nanofibers was only 1.45 V (Fig. 4B). The voltage output of the device made of AuNC/PVDF nanofibers was increased by 12.6-fold relative to the case of pristine PVDF nanofibers, indicating a significantly enhanced sensitivity of the AuNC/PVDF nanofibers for tactile sensing. This difference can be attributed to a greater β phase content caused by the inclusion of AuNCs in the PVDF nanofibers. Besides, introducing metallic nanoparticles into a polymer host increases the dielectric constant of the polymer as a result of the interfacial polarization phenomenon. Fig. 4, C and D, shows the outputs in terms of open-circuit voltage and current when the device made of the AuNC/PVDF nanofibers was subjected to cycled compressive loading at 2, 3, and 5 Hz, respectively. The peak voltage and current were insensitive to the frequency of variation within the experimental range, which is consistent with the observation of a previous report.[28] The highest voltage and current outputs of the device were 18.1, 18.2, and 18.9 V and 28.1, 28.3, and 27.4 nA, at a loading frequency of 2, 3, and 5 Hz, respectively, suggesting that this device could output electrical signal stably at a number of frequencies for a relatively long period of time.

We then evaluated the capability of the AuNC/PVDF nanofibers to detect NIR light by converting light to electrical signal through photothermal heating. Under the irradiation of an 808-nm diode laser, the temperature rise in the mat of AuNC/PVDF nanofibers was measured using an infrared (IR) camera. For comparison, a nonwoven mat of the pristine PVDF nanofibers were also tested. As shown in Fig. 5A, the temperature of the pristine PVDF nanofibers remained at 23.7 °C after 60 s of irradiation. Because of the lack of a photothermal agent, the pristine PVDF nanofibers could not directly absorb visible and NIR light, preventing the conversion from light to heat. However, within 60 s of irradiation, the

nonwoven mat of AuNC/PVDF nanofibers showed a drastic increase in temperature from 20 to 73.9 °C, due to the presence of AuNCs (Fig. 5B). The uniform distribution of AuNCs in the mat of PVDF nanofibers was also confirmed. We observed similar temperature rise profiles at different locations of a nonwoven mat made of the AuNC/PVDF nanofibers upon 60 s of irradiation with the 808-nm laser (Fig. 5C), suggesting that the AuNCs were uniformly distributed and dispersed in the nanofibers during the electrospinning process. Due to LSPR-assisted heating, the nonwoven mat of AuNC/PVDF nanofibers could effectively convert NIR light to heat with an efficiency much greater than that of PVDF alone (Fig. 5D). Moreover, the nonwoven mat of AuNC/PVDF nanofibers also exhibited good durability under extended laser irradiation. As shown in Fig. 5E, there was no significant change to the photothermal conversion efficiency after 640 rounds of irradiation, suggesting that the irradiation did not alter the plasmonic features of the AuNCs. This stability would ensure a long working life span for the device.

Fig. 6A and B shows the temperature increase/decrease profiles in a nonwoven mat of the AuNC/PVDF nanofibers when the sample was subjected to on/off irradiation cycles using the 808-nm diode laser at a power density of 0.2 W/cm^2. The rise in temperature (ΔT) could reach up to 51.3 °C when subjected to laser irradiation, and then decreased slowly to zero after the NIR light was turned off. As shown in Fig. 6C, the highest voltage output from the device was *ca.* 7.2 V, which was smaller than that of the piezoelectric cell shown in Fig. 4A, but was on par with the device reported in literature.[29] For the device reported in literature, however, a light absorption layer had to be added in order to transfer NIR light to heat, which may limit the scope of application. As a major advantage, the mat of AuNC/PVDF nanofibers could serve as the adsorption layer owing to the incorporation of AuNCs. The hybrid device can directly response to NIR irradiation by transferring light to heat and then electric signal by integrating the unique photothermal feature of AuNCs and the pyroelectricity of PVDF. The high sensitivity of this device toward NIR light could lead to the development of photodetectors. Fig. 6D shows the voltage outputs from a device when it was subjected to tactile force and NIR irradiation simultaneously, with a maximum output voltage as high as 25.5 V. This value was greater than that of an individual piezoelectric or pyroelectric cell. This result demonstrates that the hybrid device can also simultaneously detect tactile and NIR light stimulations.

Conclusions

In summary, we have demonstrated the fabrication of a hybrid device made of electrospun PVDF nanofibers and AuNCs, which can be used for simultaneous detection of both tactile and NIR light stimulations. The incorporation of AuNCs into the PVDF nanofibers also increased the content of β phase, leading to more favorable piezoelectric response. In addition, the strong optical absorption of AuNCs gave the PVDF nanofibers a new capability to convert light to heat and then electric signal, realizing the effective detection of NIR light. The voltage output of the device based on the AuNC/PVDF nanofibers could reach 18.3 V under the tactile force, which was more than 10 folds greater than that of the pristine PVDF nanofibers. Furthermore, a voltage output of 7.2 V was obtained when the device was subjected to the repeated on/off irradiation cycles using an 808-nm diode laser at a power density of 0.2 W/cm^2. Taken together, this work provides a platform nanomaterial for

developing PVDF-based sensors integrated with both piezoelectric and pyroelectric capabilities for applications related to tactile sensing and NIR light detection.

Supplementary Material

Refer to Web version on PubMed Central for supplementary material.

Acknowledgements

This work was supported in part by a grant from the National Institutes of Health (R01 EB020050) and startup funds from the Georgia Institute of Technology. As jointly supervised PhD candidates from Donghua University, H.L. and T.W. were also partially supported by fellowship awards from China Scholarship Council. We thank Dr. Chen Huang for providing the ITO-coated plastic films.

References

(1). Gogurla N, Sinha AK, Santra S, Manna S, and Ray SK, Sci. Rep, 2014, 4, 6483. [PubMed: 25255700]

(2). Yang X, Yang M, Pang B, Vara M, and Xia Y, Chem. Rev, 2015, 115, 10410–10488. [PubMed: 26293344]

(3). Yavuz MS, Cheng Y, Chen J, Cobley CM, Zhang Q, Rycenga M, Xie J, Kim C, Song KH, Schwartz AG, and Xia Y, Nat. Mater, 2009, 8, 935–939. [PubMed: 19881498]

(4). Wang Z, and Song J, Science, 2006, 312, 242–246. [PubMed: 16614215]

(5). Neese B, Chu B, Lu SG, Wang Y, Furman E, and Zhang Q, Science, 2008, 321, 821–823. [PubMed: 18687960]

(6). Martins P, Lopes AC, and Lanceros-Mendez S, Prog Polym Sci, 2014, 39, 683–706.

(7). Chinnappan A, Baskar C, Baskar S, Ratheesh G, and Ramakrishna S, J. Mater. Chem. C, 2017, 5, 12657–12673.

(8). Sharma M, Madras G, and Bose S, Phys. Chem. Chem. Phys, 2014, 16 14792–147909. [PubMed: 24922560]

(9). Lee C, and Tarbutton J. Smart. Mater. Struct, 2014, 23, 095044–095051.

(10). Chen X, Shao J, An N, Li X, Tian H, Xu C, and Ding Y, J. Mater. Chem. C, 2015, 3, 11806–11814.

(11). Divya S, and Hemalatha J, Eur. Polym. J, 2017, 88, 136–147.

(12). Fang J, Wang X, and Lin T, J. Mater. Chem, 2011, 21, 11088–11091.

(13). Abolhasani M, Shirvanimoghaddam K, and Naebe M, Compos Sci Technol, 2017, 138, 49–56.

(14). Garain S, Jana S, Sinha T, and Mandal D, ACS Appl. Mater. Interfaces, 2016, 8, 4532–4540. [PubMed: 26829464]

(15). Tsutsumi N, Kosugi R, Kinashi K, and Sakai W, ACS Appl. Mater. Interfaces, 2016, 8, 16816–16822. [PubMed: 27309153]

(16). Mandal D, Henkel K, and Schmeiber D, Phys. Chem. Chem. Phys, 2014, 16, 10403–10407. [PubMed: 24733435]

(17). Li J, Yang M, Sun X, Yang X, Xue J, Zhu C, Liu H, and Xia Y, Angew. Chem. Int. Ed, 2016, 128, 14032–14036.

(18). Huang X, Jiang P, and Xie L, Appl. Phys. Lett, 2009, 95, 242901.

(19). Wang W, Zhang S, Srisombat L, Lee TR, and Advincula RC, Macromol. Mater. Eng, 2011, 296, 178–184.

(20). Wang G, Deng Y, Xiang Y, and Guo L, Adv. Funct. Mater, 2008, 18, 2584–2592.

(21). Skrabalak S, Au L, Li X, and Y. Xia. Nat. Protoc, 2007, 2, 2182–2190.

(22). Sun X, Kim J, Gilroy KD, Liu J, König TA, and Qin D. ACS Nano, 2016, 10, 8019–8025. [PubMed: 27458731]

(23). Yang M, Huo D, Gilroy KD, Sun X, Sultan D, Luehmann H, Detering L, Li S, Qin D, Liu Y, and Xia Y, ChemNanoMat, 2017, 3, 44–50.

(24). Yang M, Kyle G, and Y. Xia. Part. Part. Syst. Charact, 2017, 34, 1600279.

(25). Peña-Rodríguez O, Caro M, Rivera A, Olivares J, Perlado JM, Caro A, Opt. Mater. Express, 2014, 4, 403.

(26). Kelly K, Coronado E, Zhao L, and Schatz G, J. Phys. Chem. B, 2003, 107, 668–677.

(27). Lovigner AJ, Science, 1983, 220, 1115–1121. [PubMed: 17818472]

(28). Kulkarni E, Heussler S, Stier A, Fernandez I, Andersen H, Toh C, and Ozyilmaz B, Adv.Optical Mater, 2015, 3, 34–38.

(29). Yang Y, Zhang H, Zhu G, Lee S, Lin Z-H, and Wang ZL, ACS Nano, 2013, 7, 785–790. [PubMed: 23199138]

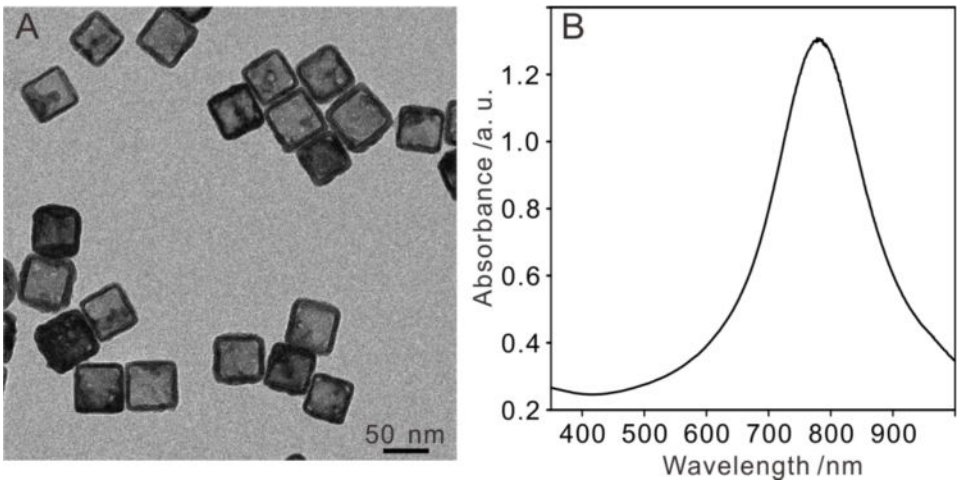

Fig. 1.

(A) A typical TEM image of the AuNCs before incorporation into the PVDF nanofibers and (B) UV-vis-NIR spectrum recorded from an aqueous suspension of the AuNCs.

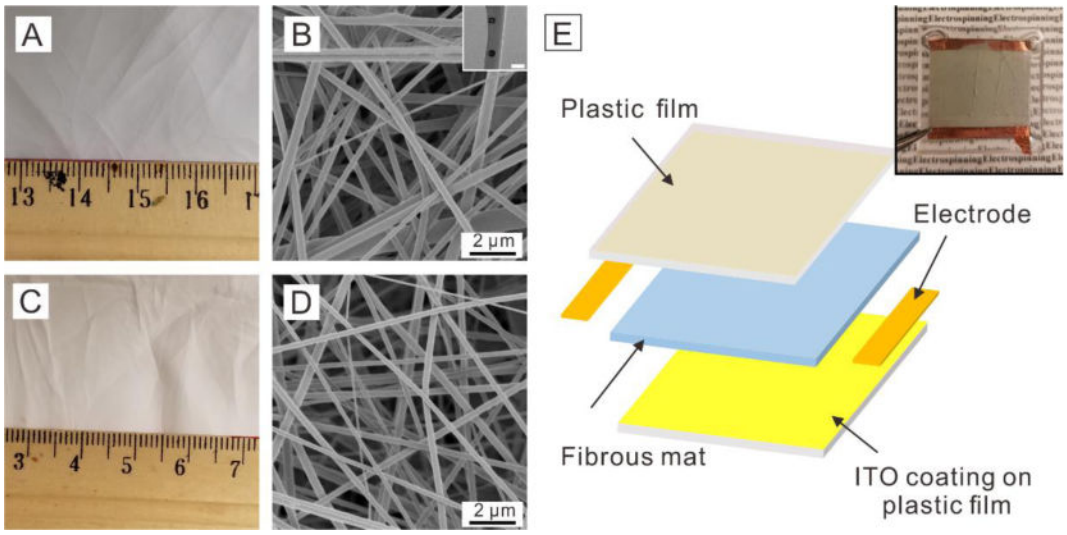

Fig. 2.

Photograph and SEM images of a nonwoven mat of (A, B) the AuNC/PVDF and (C, D) pristine PVDF nanofibers, respectively. The inset in (B) shows a TEM image taken from one of the nanofibers (scale bar: 50 nm). (E) Schematic drawing of a sensing device that was constructed using an ITO-coated plastic film (upper layer), a nonwoven mat of AuNC/PVDF nanofibers (middle layer), and another ITO-coated plastic film (bottom layer). A photograph of the device is shown at the upper right corner.

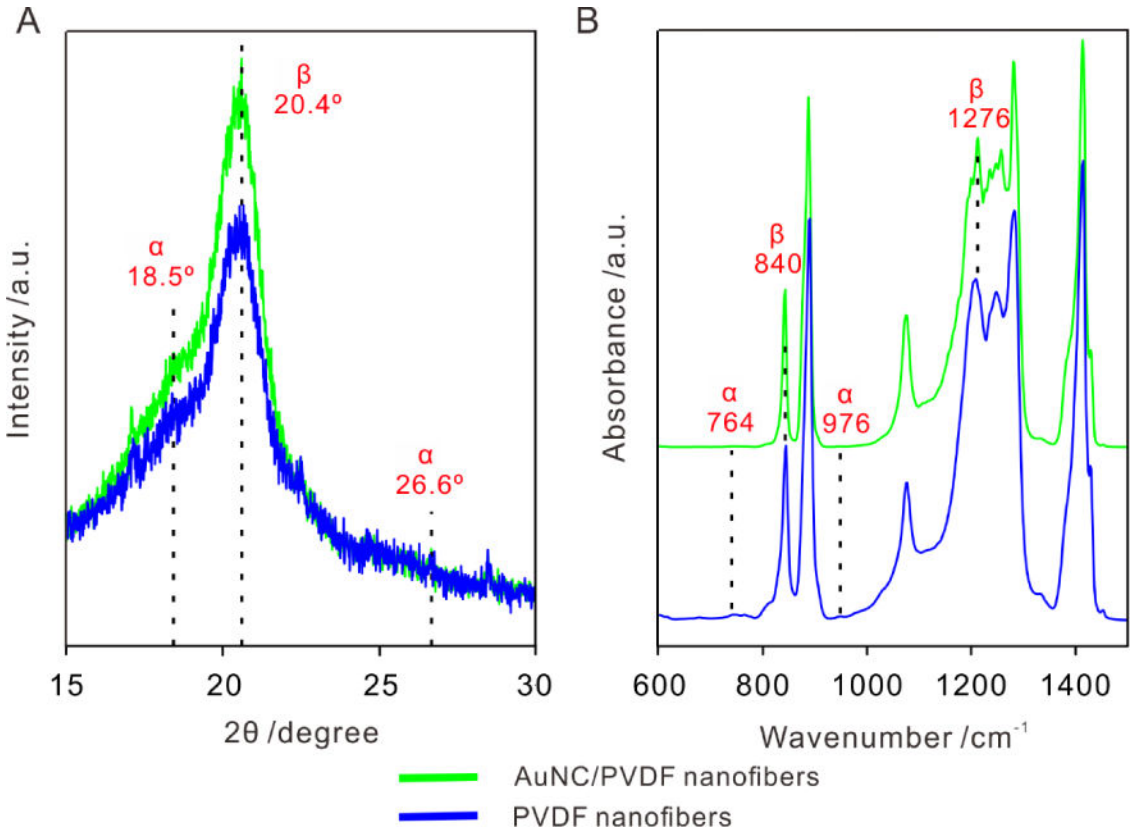

Fig. 3.

(A) XRD patterns and (B) FT-IR spectra recorded from nonwoven mats of the AuNC/PVDF and pristine PVDF nanofibers, respectively. The color scheme applies to both XRD patterns and FT-IR spectra.

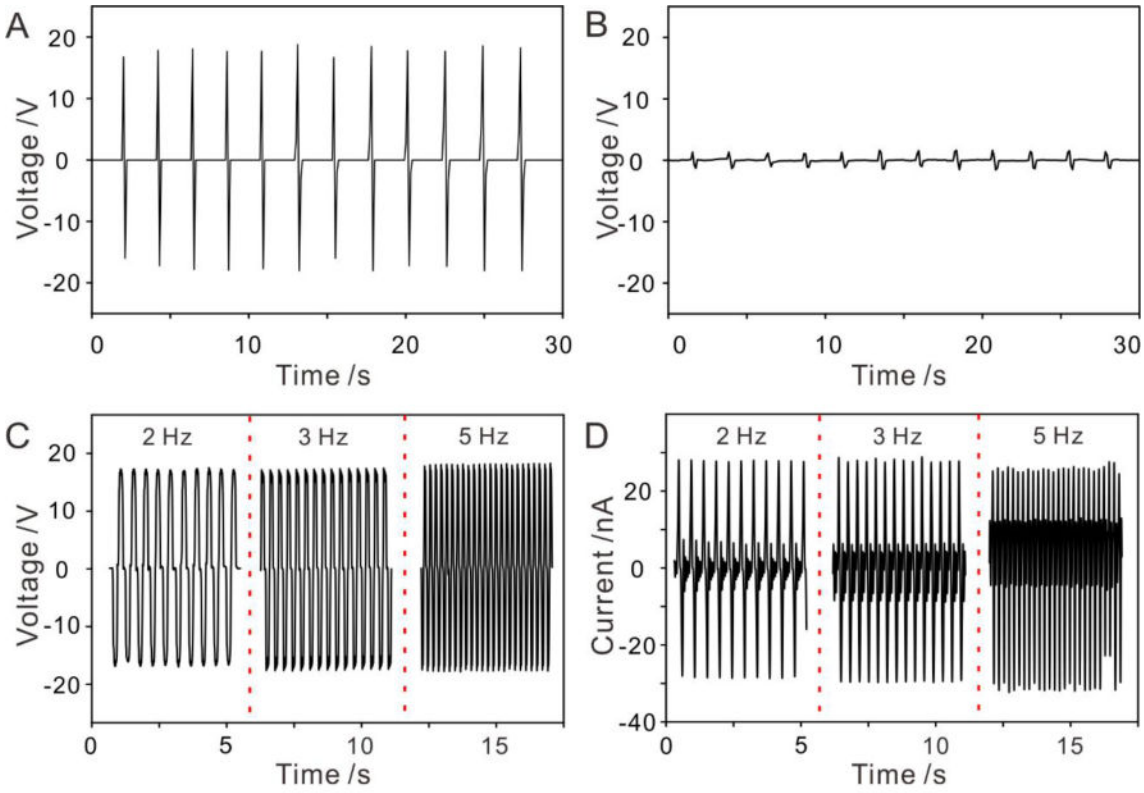

Fig. 4.

Voltage outputs from the devices fabricated using a mat of (A) the AuNC/PVDF nanofibers and (B) the pristine PVDF nanofibers, respectively, when they were subjected to a repeated compressive force. Outputs in terms of (C) open-circuit voltage and (D) current during a test performed at different frequencies using a device made of the AuNC/PVDF nanofibers.

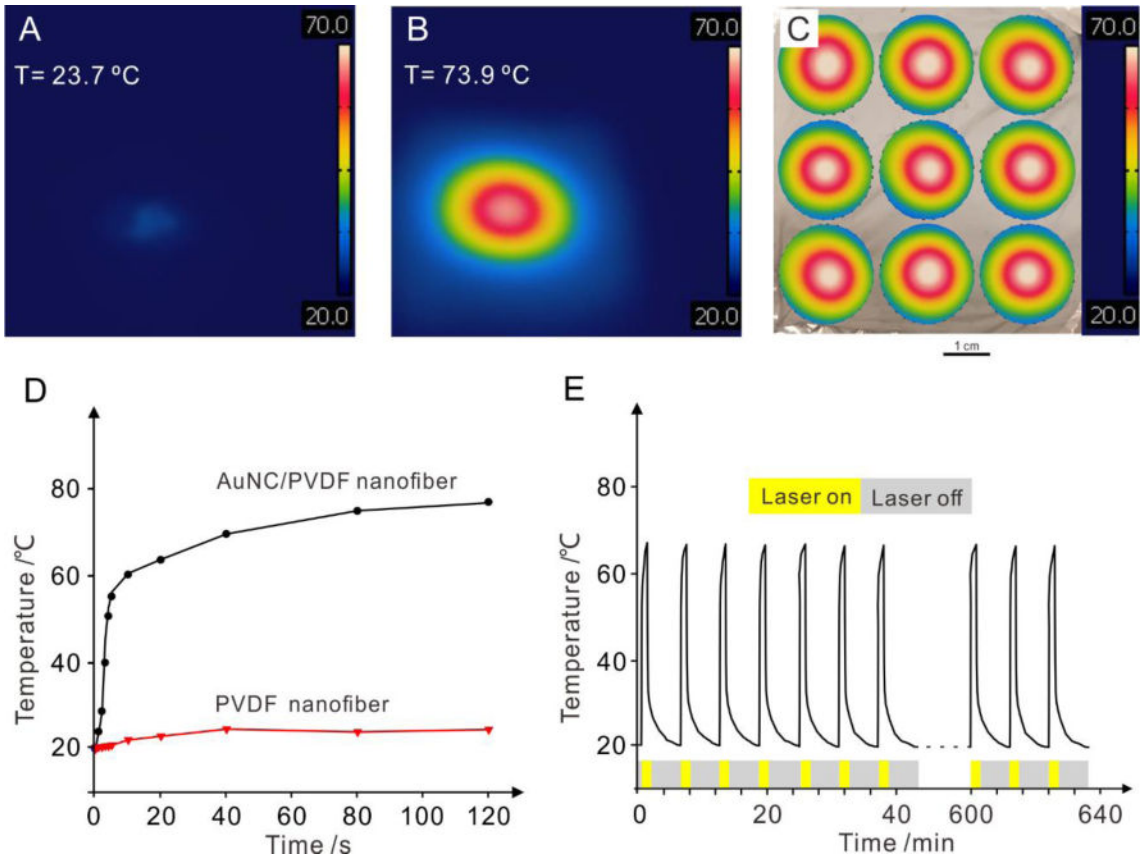

Fig. 5.

IR camera images showing the temperatures in the nonwoven mats of (A) pristine PVDF nanofibers and (B) AuNC/PVDF nanofibers after 60 s of irradiation with an 808-nm laser at a power density of 0.2 W/cm^2. (C) IR camera images showing the temperatures at different positions in a mat of AuNC/PVDF nanofiber after 60 s of irradiation with the 808-nm laser at a power density of 0.2 W/cm^2. (D) Comparison of the temperature rise recorded from the mats of AuNC/PVDF nanofibers and pristine PVDF nanofibers, respectively, upon the irradiation by the 808-nm laser at a power density of 0.2 W/cm^2 for 2 min. (E) Plots showing the changes of temperature in the mat of AuNC/PVDF nanofibers upon repeated irradiation by the 808-nm laser at a power density of 0.2 W/cm^2.

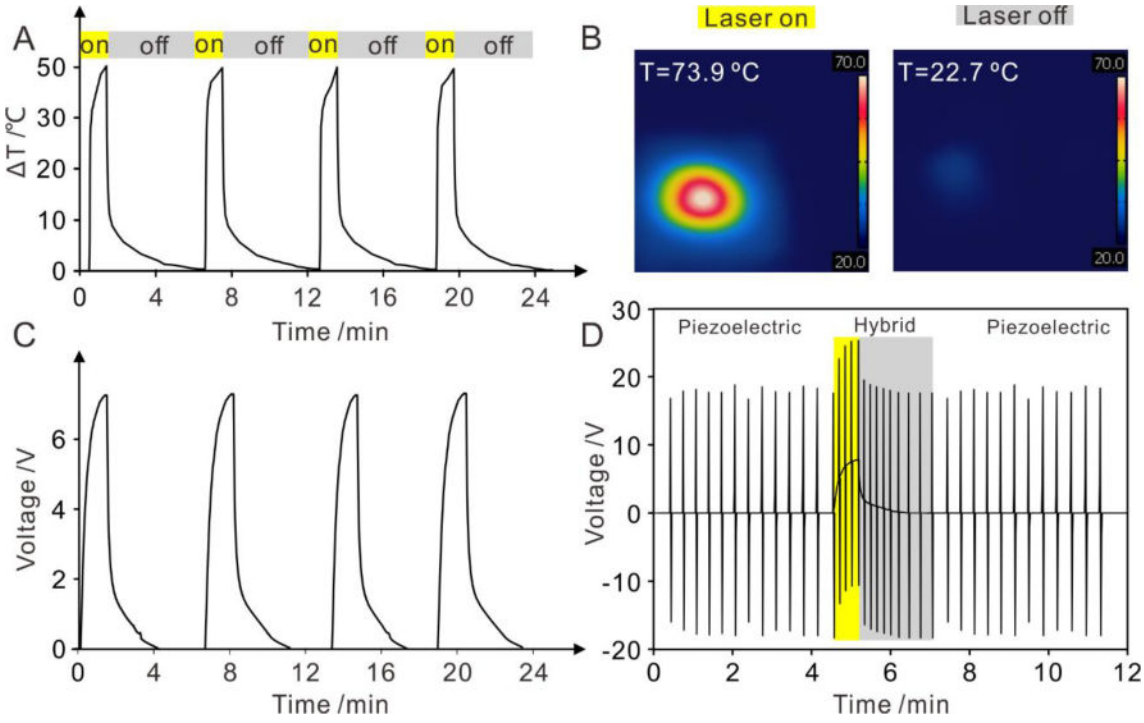

Fig. 6.

(A) Cyclic changes in temperature and (B) IR camera images showing the temperature rise and drop in a nonwoven mat of AuNC/PVDF nanofibers when it was (left) exposed to and (right) blocked from the 808-nm laser at a power density of 0.2 W/cm^2. (C) Pyroelectric response of a device fabricated using a nonwoven mat of AuNC/PVDF nanofibers when it was exposed to and blocked from the 808-nm laser at a power density of 0.2 W/cm^2. (D) Voltage outputs from a device fabricated using a nonwoven mat of AuNC/PVDF nanofibers when it was subjected to both tactile and NIR light stimulations.